Effects of Alloyed Metal of $Cu_3X(111)$ on Controlling O-H and α-C-H Bond Cleavages for Ethanol Dehydrogenation (X=Zr, In, Ag, Au)

Han Xu,[a] Ruitao Wu,[b] Minhua Zhang,[a] Bei Miao,[a] Yifei Chen,[a] and Lichang Wang[*,a,b]

[a]Key Laboratory of Ministry of Education for Green Chemical Technology and the R & D Center for Petrochemical Technology, Tianjin University and Collaborative Innovation Center of Chemical Science and Engineering, Tianjin 300072, China;
[b]Department of Chemistry and Biochemistry and the Materials Technology Center, Southern Illinois University, Carbondale, Illinois 62901, United States.

Abstract

Economically advantageous Cu-based catalysts have been widely used for a great number of reactions related to ethanol. However, serious obstacles still remain, such as the high reaction energy barrier and low selectivity for the first step of the dehydrogenation of ethanol. In this study, O-H and α-C-H bond cleavages in ethanol on a $Cu_3X(111)$ surface (X= Zr, In, Ag, Au) were carried out using DFT to explore the effect of alloying on the selective and effective dehydrogenation of ethanol. $Cu_3Zr(111)$ was found to have superior catalytic performances for dehydrogenation with significantly low reaction barriers for both O-H bond cleavage (0.13 eV) and α-C-H bond cleavage (0.73 eV), which are much lower than the results on Cu(111). Thus this work indicates that alloying Zr can selectively break the O-H bond of ethanol, which cannot be accomplished using Pt, Pd, or Cu catalysts. Meanwhile, through PDOS analysis, Mülliken charge analysis, and d-band center analysis, there are two key factors that contribute to the great improvements on the dehydrogenation catalytic activities of $Cu_3X(111)$. Firstly, the specific inherent properties of the second alloyed metal X, including the d-band center, are crucial to the adsorption and activation of ethanol on surfaces. Secondly, the electronic distribution on the surfaces resulting from the difference of electronegativity between the metals Cu and X is associated with the dehydrogenation reaction barrier. More electron density around the Cu atoms on these surfaces is more beneficial for dehydrogenation reactions, especially when H atoms were adsorbed stably on the Cu sites.

Introduction

In the search for a comparable energy source to replace traditional fossil fuels, ethanol as bio-renewable fuel has become a promising contender.[1, 2] Ethanol can be used to produce hydrogen for hydrogen fuel cells[3-5] and can also be utilized directly in ethanol fuel cells.[6, 7] In addition, ethanol is a starting material in the synthesis of products including acetaldehyde, ethylene, acetic acid, ethyl ester, and ethyl acetate.[8, 9] All of the utilization of ethanol involve the decomposition of ethanol on catalysts surfaces and a number of metal catalysts was found to decompose ethanol effectively.[10-35] Among a tremendously large reaction network of ethanol decomposition,[7, 14, 36-38] the dehydrogenation of ethanol is the first step and considered of great importance due to its significance in affecting the reaction pathways of product formation.

There are three kinds of hydrogen atoms in ethanol: hydroxyl-H (denoted as *o*-H in this work), α-H, and β-H.[39, 40] Previous studies of ethanol dehydrogenation on Pd(111) and Pt(111) surfaces illustrated that it is easier to break the α-C-H bond.[41, 42] Our previous Density Function Theory (DFT) studies showed that the bonding energy of β-C-H is the largest (4.28 eV), followed by O-H (4.23 eV), and α-C-H is the smallest (3.92 eV), which also suggests that ethanol dehydrogenation is most likely to occur *via* α-C-H bond cleavage.[8] As we expect, the product CH_3CHOH of ethanol dehydrogenation via α-C-H cleavage will trigger a different decomposition pathway than the product CH_3CH_2O that is via the O-H cleavage. Therefore, it is of great importance to design catalysts for higher catalytic activity and selectivity for ethanol dehydrogenation to ethoxy. Simultaneously, the mechanism behind these catalytic performances for different types of ethanol dehydrogenation deserves in-depth exploration.

As a cheap metal catalyst, in comparison to the Pt,[43-50] Pd,[51-56] Ir,[57, 58] and Au[59-63] nanoparticles, copper-based catalysts have often been studied for ethanol oxidation and decomposition reactions.[64-68] Besides, for partial ethanol oxidation to acetaldehyde, copper-based catalysts also present a wide utilization, which shows more desirable selectivity.[69, 70] Wang et al. demonstrated that, through the study of ethanol dehydrogenation on Cu(111) and Cu(110), the O−H bond of ethanol was broken at a lower temperature to form alkoxy intermediates while the α-C−H bond was broken at higher temperature to form aldehyde.[71] Our DFT studies also indicated that the O-H bond scission may become as competitive as the α-C-H bond scission on the Cu(111) surface.[8] As such, we investigated different Cu-based bimetallic catalysts using DFT calculations and compared their catalytic performances for the dehydrogenation of ethanol via O-H and α-C-H bond scissions to illustrate the function of various secondary metals that may be similar to the polarization effect[72] or ligands in catalysis.[73-75]

The choices of the secondary alloyed metals were made within the same period as Pd and among the same group of Cu (see Fig.1). In the same period as Pd, we firstly selected Zr as the second metal to form $Cu_3Zr(111)$. Zirconia has been frequently used in acid-base catalysis or as catalyst support.[76-79] In this work, we further explored the effect of Zr on ethanol dehydrogenation from the aspect of an alloyed metal. CuZr system is a kind of typical glassy alloy, which owns special material properties, such as high strength and corrosion resistance,[80-82] but its catalytic activity still remains unclear from the theoretical point of view and is worth exploring. We also selected In as the second alloyed metal to form $Cu_3In(111)$, which aims to achieve a completely different bimetallic catalyst from $Cu_3Zr(111)$, specifically in terms of the

surface electronic distribution. Onyestyak et al. found that when doped with In_2O_3, Cu exhibited an improved catalytic performance for acetic acid hydrogenation to ethanol due to the existence of the Cu_2In phase.[83-86] Liu et al. investigated computationally the reaction network of ethanol formation from acetic acid on $Cu_2In(100)$.[87] Their results show that In may have a positive effect on O-H bond formation. Hence, $Cu_3In(111)$ was selected for the first step of ethanol dehydrogenation here and compared with the results on $Cu_3Zr(111)$ to clarify the surface composition and charge distribution effect on the catalytic activity of ethanol dehydrogenation.

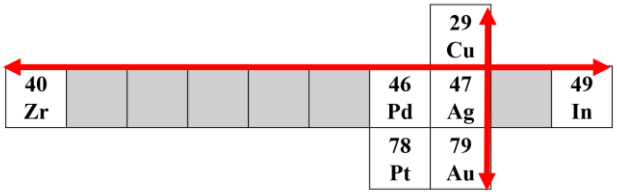

Fig. 1 Selections for the second alloyed metal X in $Cu_3X(111)$ (X= Zr, In, Ag, Au).

Furthermore, Ag and Au were selected to form $Cu_3Ag(111)$ and $Cu_3Au(111)$, respectively. CuAg bimetallic catalysts have been widely utilized in electrochemical CO_2 reduction,[88] hydroxylation of benzene via C-H bond cleavage,[89] NO reduction and so on.[90] The specific catalytic performances of Cu-Ag bimetallic catalysts on ethanol dehydrogenation are still unclear. On the other hand, Cu-Au bimetallic catalysts were revealed to be able to catalyze selective oxidation of ethanol to acetaldehyde when prepared by redox method and supported on SiO_2,[91] and Do et al. compared catalytic activity of ethanol dehydrogenation on calcined Cu, Ag, Au metals supported on TiO_2 and illustrated that the activation energy of ethylene formation from ethanol lowers from Au to Cu to Ag.[92] In this work, a DFT study on the alloy catalysts $Cu_3Ag(111)$ and $Cu_3Au(111)$ for ethanol dehydrogenation was carried out and the results have

been compared with the other bimetallic catalysts being studied.

Methodology

The Face Centered Cubic (FCC) structures of Cu_3X (X= Zr, In, Ag, Au) were used as model structures in this study so that comparisons with our previous work can be made directly.[13] Since Cu, Ag, and Au are all FCC structures, we expect that Cu_3Ag and Cu_3Au with fcc structures may be synthesized readily. On the other hand, the model FCC structures of $Cu_3Zr(111)$ and $Cu_3In(111)$ may be more challenging to synthesize as Zr is a body centered cubic structure and In is a simple tetragonal structure. However, our study will provide a valuable insight into further studies of using more realistic models and different concentrations of X.

All calculations were performed within DFT as implemented in the program package of DMol^3.[93, 94] The exchange-correlation interaction was described by the Generalized Gradient Approximation (GGA) and the Perdew-Burke-Ernzerhof (PBE) functional.[95] A double-numerical basis set with polarization functions (DNP) was used. Spin unrestricted DFT calculations were carried out. The convergence criteria included threshold values of 2×10^{-5} Ha, 0.004 Ha/Å, and 0.005 Å for energy, Max. force, and Max. displacement, respectively. Self-Consistent-Field (SCF) density convergence threshold value of 1×10^{-5} eV was used, and a Fermi smearing of 0.005 Ha was employed. Meanwhile, a DIIS size of 6 was also used to enhance the calculation speed. Similar technical details have been reported in our previous work.[8, 64, 96]

The Cu_3X crystal structure was built by substituting the Cu atom on vertices of the original Cu crystal cell with atom X, and then optimized.[8] Each alloyed metal used different proper

cutoff values in the geometry optimization process. For Zr and In, 4.6 Å and 4.4 Å respectively, and 4.0 Å for Ag and Au. After optimization, the lattice parameters for Cu_3Zr, Cu_3In, Cu_3Ag, and Cu_3Au were 3.946 Å, 3.867 Å, 3.814 Å, and 3.812 Å respectively. The experimental measurement of lattice parameter for pure copper is 3.623 Å.[97] After alloying with other metal atoms, the lattice parameters of Cu_3X are all increased to some extent. The resulting $Cu_3X(111)$ surface was cleaved from the optimized Cu_3X crystal structure. The periodic (4×4) supercell surface model with three layers of atoms was constructed. Furthermore, the atoms in the two bottom layers were fixed and the remaining atoms were fully relaxed during optimization (Fig.2). We mention that calculations were also made using a four-layer model with the top two layers were allowed to relax as well as a five-layer model with the top three layers were allowed to relax to test the three-layer model using Cu_3Ag and Cu_3Zr systems. The adsorption energy of ethanol on $Cu_3Zr(111)$ using four-layer model was found to be -0.11 eV more stable than that from the three-layer model. While the adsorption of ethanol on both systems and dehydrogenation on Cu_3Ag were found no drastic changes in comparison to the results from the three-layer model, the formation of ZrH hydride changes the surface structure of model catalysts greatly and the reconstructed surface makes the transition state search unsuccessful. This presents a serious challenge and more systematic work on the proper representation of model CuZr catalysts is in progress. Nevertheless, the constrained model for $Cu_3Zr(111)$ system provides important insights into the performance of this bimetallic catalyst and suggests that small concentration of Zr seems to be a better choice. The other parameters, such as adsorption configuration and bond distances, remain unchanged. To save computing time, the three-layer model was employed. A ($2\times2\times1$) k-point mesh was utilized to sample the surface Brillouin zone, and a 15

Å vacuum was introduced between the repeated slabs along the z-direction. We note that the convergence test of the mesh points was made and the results are shown in Tables S1 and S2 of supporting information. The even mesh was also used by others.[98] The adsorption energy of ethanol on $Cu_3Zr(111)$ using a (3×3×1) k-point mesh was found to be -1.04 eV, which is about 0.07 eV lower.

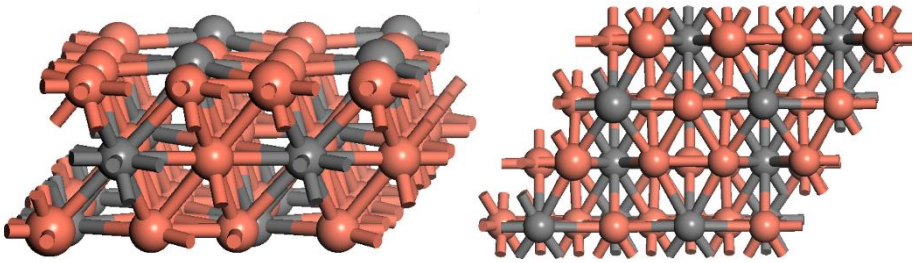

Fig.2 Periodic (4×4) supercell surface model of $Cu_3X(111)$ (X= Zr, In, Ag, Au). Color code: Cu (orange) and X= Zr, In, Ag, or Au (grey).

The isolated molecule was optimized in a vacuum space of 15 Å by using the core treatment of all electron. The cutoff values kept the same with those of different bulks. Other calculation parameters were consistent with those mentioned above. This is the same method as our previous calculations for ethanol[8, 9] and other isolated molecules.[99, 100] Furthermore, the adsorbate species were optimized on different kinds of slabs. All of the adsorption species were fully relaxed and a lack of imaginary frequencies was confirmed. The adsorption energies were calculated as:

$$\Delta E_{ad} = E_{adsorbate/slab} - (E_{adsorbate} + E_{slab}), \quad (1)$$

where $E_{adsorbate}$, E_{slab}, and $E_{adsorbate/slab}$ are the total energy of the gas phase adsorbate species, $Cu_3X(111)$ surface, and adsorbate on $Cu_3X(111)$ surface, respectively. Furthermore, all the calculated energies were ZPE corrected:

$$\Delta E_{ad}^{0} = \Delta E_{ad} + \sum_j \frac{hv_j}{2} - (\sum_m \frac{hv_m}{2} + \sum_n \frac{hv_n}{2}), \quad (2)$$

where v_j, v_m, v_n are the frequency of jth vibrational modes of the adsorption configuration on $Cu_3X(111)$ surface, mth vibrational modes of $Cu_3X(111)$ bulk and nth vibrational modes of adsorbate, h is Planck's constant. ΔE_{ad}^{0} is ZPE corrected adsorption energy.

We also performed single point DFT-D2 calculations to investigate the impact of long-range dispersion to the adsorption energy. The results are provided in Table S3 of the supporting information. Our results show that the relative stability barely changes but the adsorption energy is increased in all cases by about 0.5 eV when dispersion is considered. As such, it seems that the DFT-D method[101, 102] will not affect the results for strong chemisorption of reactants.

Transition states searches were performed using a generalization of the linear synchronous transit (LST) method for periodic systems combined with a quadratic synchronous transit (QST) method.[103] Only one imaginary frequency was permitted in each TS after the searching process, which was characterized by vibrational analysis. The activation barrier and reaction energy of each reaction step was calculated as:

$$\Delta E_a = E_{TS} - E_{IS}, \quad (3)$$

$$\Delta E = E_{FS} - E_{IS}, \quad (4)$$

where the energies of reactant (E_{IS}), transition state (E_{TS}), and product (E_{FS}) are all ZPE corrected:

$$\Delta E_a^0 = \Delta E_a + \sum_j \frac{hv_j^{\neq}}{2} - \sum_j \frac{hv_j}{2}, \quad (5)$$

$$\Delta E^0 = \Delta E + \sum_k \frac{hv_k}{2} - \sum_j \frac{hv_j}{2}, \quad (6)$$

where ΔE_a^0 and ΔE^0 are ZPE corrected energy barriers and reaction energies, $v_j^{\neq}$, v_j and v_k are the frequency of vibrational modes of the TS, IS and FS, respectively. Additionally, all

the vibrational frequencies were obtained by the finite difference of the atomic positions. We note that the finite difference calculations of harmonic vibrational frequencies were shown to be rather accurate.[104]

The pathways of H dissociation were designed by connecting the most stable reactants and products with their relatively lowest energies. It is also ensured that the vibrational direction of the only imaginary frequency of the transition state is consistent with the direction of H dissociation. This practice is the same as our previous work in the search of transition states.[8, 99, 105-109]

The Mülliken charges of atoms were also obtained from our DFT calculations using the default parameters. We note that the Mülliken charges of atoms were also be used by others[87, 110] and ourselves[105] to correlate the effect of charge transfer on the catalytic activities of metallic or metal oxide systems and interesting observations were made. Meaningful correlations were observed previously[87, 105, 110] and in this work. The Mülliken charges of the surface Cu atom on $Cu_3Zr(111)$, $Cu_3Ag(111)$, and $Cu_3In(111)$ are -0.224, -0.008, and 0.296 electrons, respectively. The charges of the surface X atom are 0.584 (Zr), 0.018 (Ag), and -0.146 (In) electrons. In the case of $Cu_3Ag(111)$, the Mülliken charges of the surface Cu and Au atoms are 0.030 and -0.096 electrons, respectively. The Mülliken charges can clearly indicate the direction of charge transfer between two kinds of metal atoms on surfaces, and the relative extent of charge transfer can also be qualitatively compared.

Results and Discussion

In this work, two kinds of the ethanol dehydrogenation reactions: O-H and α-C-H bond cleavages, and ethanol adsorption on four different $Cu_3X(111)$ surfaces with X= Zr, In, Ag, Au

were studied. The specific geometric and electronic effects were also investigated. In what follows, we first present the results of the ethanol adsorption, followed by the O-H bond cleavage, $CH_3CH_2OH \rightarrow CH_3CH_2O+H$, on the four $Cu_3X(111)$ surfaces.

The adsorption energies of ethanol on different sites of different surfaces are included in Table 1, which can clearly illustrate the main adsorption and reaction centers on these different alloy surfaces. We note that most of the energies reported here are ZPE corrected. Energies without ZPE corrections were only obtained for special comparison purposes and for saving computing times. In these cases, the energy reported will be explicitly stated.

Table 1 Adsorption energies of ethanol on different sites of $Cu_3X(111)$ (X=Zr, In, Ag, Au). Bolded values indicate that the adsorption sites are the more stable ones.

$Cu_3X(111)$	**Cu site (eV)**	**X site (eV)**
$Cu_3Zr(111)$	-0.27	**-0.93**
$Cu_3In(111)$	-0.21	**-0.27**
$Cu_3Ag(111)$	**-0.22**	-0.19
$Cu_3Au(111)$	**-0.24**	-0.08

DFT results of O-H bond cleavage in CH_3CH_2OH on $Cu_3X(111)$ (X= Zr, In, Ag, Au) are depicted in Fig.3, where the adsorption configurations of the reactant and products, and the transition state of the reaction, including barriers and reaction energies, are all provided. The results of O-H bond cleavage on $Cu_3Zr(111)$ in Fig.3 show that $CH_3CH_2OH \rightarrow CH_3CH_2O+H$ is strongly exothermic with a reaction energy of -1.17 eV and the reaction barrier (0.13 eV) is significantly smaller than that on Cu(111). This indicates that the O-H bond cleavage is definitely easier on $Cu_3Zr(111)$ from both a thermodynamics and a dynamics perspective. For the initial state, ethanol is adsorbed on the atop site of the Zr atom with a Zr-O distance of 2.288

Å. The adsorption energy is -0.93 eV, which is a remarkable chemical adsorption. For the transition state, CH_3CH_2O is still adsorbed on the atop of Zr atom with the Zr-O distance of 1.127 Å, and H atom moves away from the O atom of ethanol to the neighboring Cu-Cu bridge site. The distance between O and H in the transition state is 1.296 Å. When it comes to the final state, CH_3CH_2O adsorbs in a similar configuration as transition state and the Zr-O bond length is 1.927 Å. The dissociated H atom is adsorbed on the Cu-Cu bridge site with the Cu-H bonds of 1.718 and 1.713 Å. We note that these product adsorption configurations as well as those reported below are the ones leading to the lowest reaction barrier.

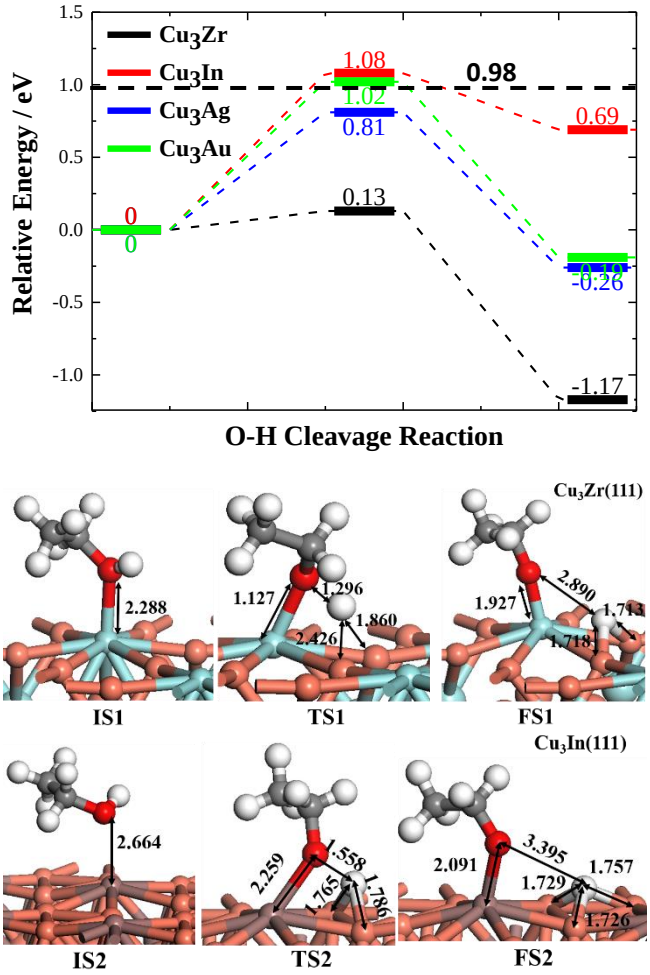

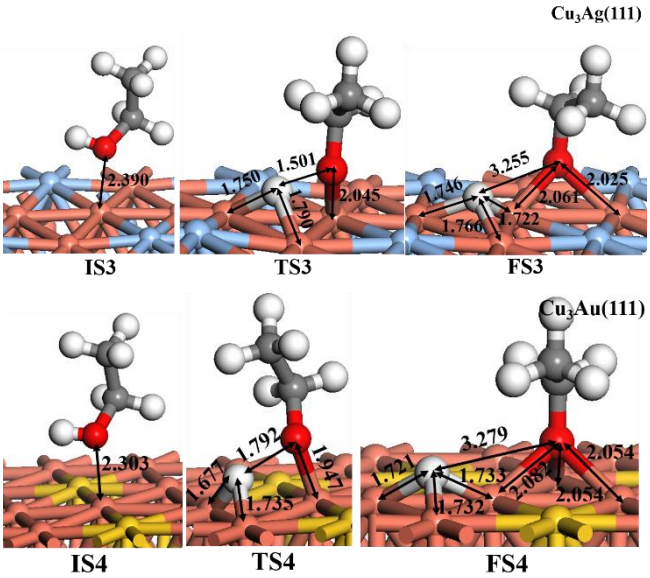

Fig.3 Structural data and energetics for the O-H cleavage of ethanol, initial states (ISs), transition states (TSs), and final states (FSs) on $Cu_3Zr(111)$ (IS1, TS1, FS1), $Cu_3In(111)$ (IS2, TS2, FS2), $Cu_3Ag(111)$ (IS3, TS3, FS3), and $Cu_3Au(111)$ (IS4, TS4, FS4). The black dotted line is the reaction barrier of O-H cleavage on Cu(111).[13] Key geometrical distances are provided in Å. Colored balls: H (white); C (grey); O (red); Cu (orange); Zr (green); In (brown); Ag (blue); Au (yellow).

The results of the O-H bond cleavage reaction on $Cu_3In(111)$ in Fig.3 clearly illustrate that the O-H bond cleavage of ethanol is further hindered on $Cu_3In(111)$ after alloying In to Cu catalysts, since the reaction barrier is 1.08 eV, which is higher than that on Cu(111). Furthermore, the reaction is noticeably endothermic with a reaction energy of 0.69 eV. The reactant ethanol is adsorbed on the atop of the In atom with an adsorption energy of -0.27 eV, which is the most stable adsorption configuration on $Cu_3In(111)$. The O-In distance is 2.664 Å. For the transition state, CH_3CH_2O species is adsorbed on the atop site of the In atom. The In-O bond length is 2.259 Å, and distances of the nearly dissociated H atom to the two closest Cu atoms are 1.765 and 1.786 Å. For the product, CH_3CH_2O is adsorbed on the atop of the In atom, and the In and O distance is 2.091 Å. The dissociated H moves to the adjacent hollow site of Cu atoms with Cu-H bonds of 1.729/1.726/1.757 Å.

As shown in Table 1, ethanol molecule adsorbs on the Cu or In site with similar strength.

The same is true for the CuAg system. Therefore, it is necessary to perform transition state search for both sites. As we would expect, these pathways will have low reactivity. Indeed, our calculated results provided in Table S4 of supporting information confirmed this. For the dehydrogenation of *o*-H of ethanol on $Cu_3Ag(111)$ (Fig.3), the results indicate that alloying Ag does not alter the O-H cleavage drastically with respect to Cu(111), since the reaction barrier is 0.81 eV, which is slightly lower than that on Cu(111) (0.98 eV).[13] The reaction is exothermic with the reaction energy of -0.26 eV (comparable to that on Cu(111), -0.21 eV)[13]. The most stable adsorption configuration of ethanol on $Cu_3Ag(111)$ is presented in Fig.3, and the adsorption energy is -0.22 eV with the distance between O and Cu of 2.390 Å. For the transition state, CH_3CH_2O is adsorbed on the Cu atom with the Cu-O bond length of 2.045 Å. The to-be-dissociated H atom is adsorbed on the neighboring Cu-Cu bridge site with the Cu and H distances of 1.750/1.790 Å. For the products, the CH_3CH_2O species is adsorbed on the Cu-Cu bridge site with the Cu-O distances of 2.061/2.065 Å, and the dissociated H is adsorbed on the hollow site of Cu atoms and forms three Cu-H bonds (1.746/1.766/1.722 Å).

When it comes to the dehydrogenation on $Cu_3Au(111)$ (Fig.3), it can be clearly seen that the reaction barrier (1.02 eV) increases after alloying Au and the reaction energy is -0.19 eV, which is slightly exothermic. This indicates that the O-H bond cleavage becomes harder on $Cu_3Au(111)$. Ethanol is still adsorbed on the atop of Cu atom with the Cu and O distance of 2.303 Å and the adsorption energy of -0.24 eV. For the transition state, it is similar to that on $Cu_3Ag(111)$. The O and H distance is 1.792 Å. For the products, the CH_3CH_2O and H species are adsorbed on two adjacent hollow site of Cu atoms. The distances of Cu atoms and the O atom of CH_3CH_2O species are 2.082/2.054/2.054 Å, and the distances of Cu atoms and the

dissociated H atom are 1.721/1.731/1.733 Å.

The comparison of O-H cleavage on the four alloyed surfaces in Fig. 3 clearly shows that the O-H bond of ethanol is more prone to break on $Cu_3Zr(111)$, but is difficult on $Cu_3In(111)$ and $Cu_3Au(111)$. Although Ag and Au are located in the same group with Cu, the O-H bond cleavage is different on $Cu_3Ag(111)$ and $Cu_3Au(111)$ surfaces, and the former is a slightly better.

The results from DFT calculations on the α-C-H bond cleavage in CH_3CH_2OH on $Cu_3X(111)$ (X= Zr, In, Ag, Au): $CH_3CH_2OH \rightarrow CH_3CHOH+H$, are presented in Fig.4, where the adsorption configurations of reactants and products and of the transition state of these reactions, including reaction barriers and reaction energies, are also provided.

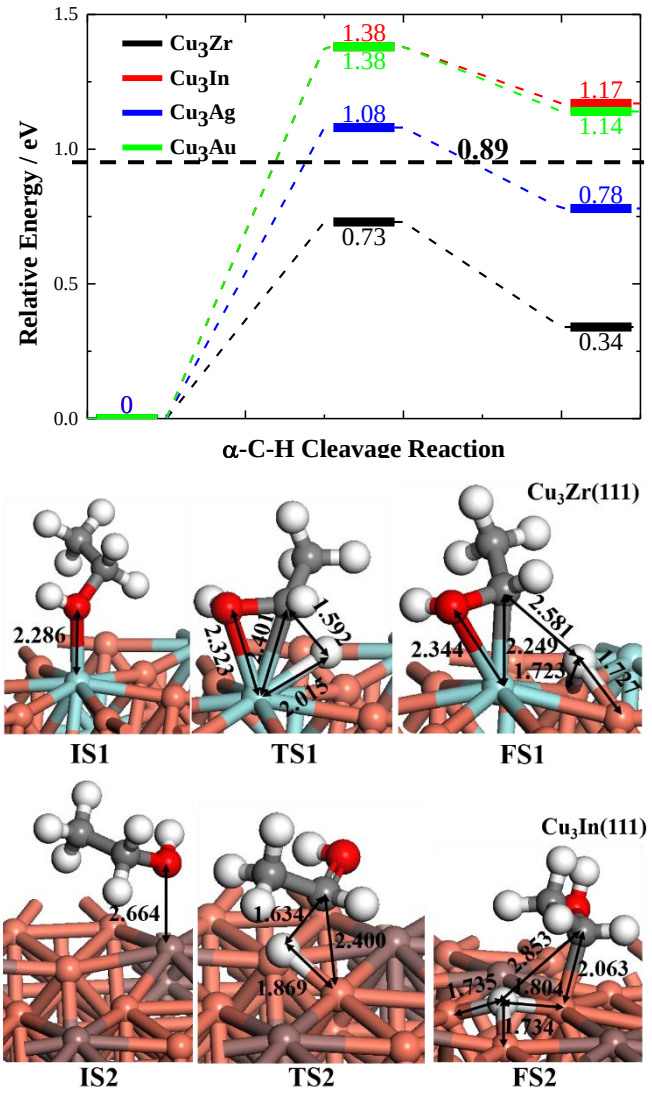

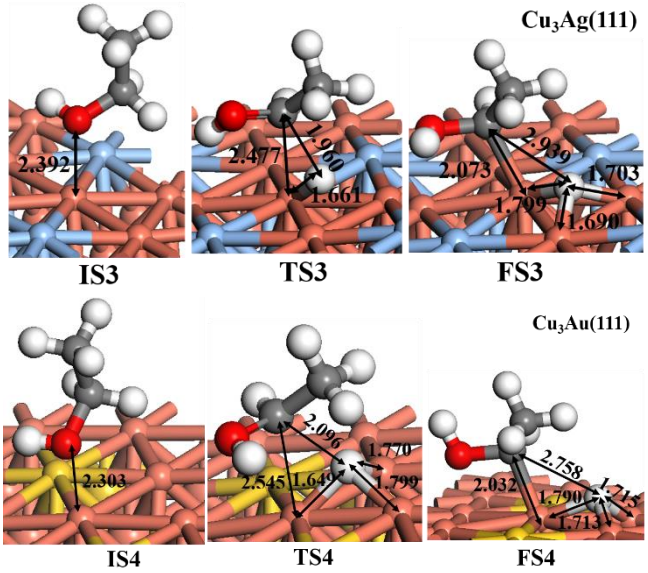

Fig.4 Energetics of the α-C-H cleavage of ethanol, initial states (ISs), transition states (TSs) and final states (FSs) on $Cu_3Zr(111)$ (IS1, TS1, FS1), $Cu_3In(111)$ (IS2, TS2, FS2), $Cu_3Ag(111)$ (IS3, TS3, FS3), and $Cu_3Au(111)$ (IS4, TS4, FS4). The black dotted line is the reaction barrier on Cu(111).[13] Key geometrical distances are provided in Å. Colored balls: H (white); C (grey); O (red); Cu (orange); Zr (green); In (brown); Ag (blue); Au (yellow).

The α-C-H bond cleavage reaction on $Cu_3Zr(111)$ as shown in Fig.4 is endothermic with a reaction energy of 0.34 eV and the reaction barrier of 0.73 eV. This indicates that alloying Cu with Zr also lowers the reaction barrier for the α-C-H bond cleavage, although the effect is not as drastic as that of the O-H cleavage. The ethanol adsorption configuration here remains the same as that of the O-H cleavage. For the transition state, the CH_3CHOH and H species are co-adsorbed to one Zr atom. Both the O and α-C atoms of CH_3CHOH bond to the Zr with a Zr-O and Zr-C bonds of 2.323/2.401 Å. The distance between the to-be-dissociated H atom and Zr is 2.015 Å. For the products, the dissociated H atom is adsorbed on the neighboring Cu-Cu bridge site, and the Cu-H bond lengths are 1.723/1.727 Å. The O and α-C atoms of CH_3CHOH are still co-adsorbed on Zr with the Zr-O and Zr-C bonds of 2.343/2.249 Å.

As for the dehydrogenation on $Cu_3In(111)$ (Fig.4),α-C-H bond cleavage becomes harder after alloying In, since the reaction barrier increases to 1.38 eV with the reaction energy of 1.17 eV. For the reactant, the adsorption configuration of ethanol remains the same as the one in the

O-H bond cleavage. For the transition state, the H is adsorbed on the atop of Cu atom with the Cu-H bond of 1.634 Å and the CH_3CHOH species is close to the to-be-dissociated H atom with the distance between the α-C and the H of 1.869 Å. The distance between the α-C of CH_3CHOH and the Cu is 2.400 Å. For the product, the H atom is located at the hollow site of Cu atoms with the length of Cu-H bonds of 1.735/1.734/1.804 Å. CH_3CHOH is adsorbed on the neighboring top of Cu atom forming the Cu-C bond. The distance between Cu and α-C is 2.063 Å.

When it comes to the reaction on $Cu_3Ag(111)$ (Fig.4), the reaction barrier (1.08 eV) increases after alloying. The reaction energy is 0.78 eV. The ethanol adsorption configuration remains the same as that in the O-H cleavage. For the transition state, the CH_3CHOH species is atop of the Cu atom with a Cu and C distance of 2.477 Å. The to-be-dissociated H atom is also bonded to the atop Cu atom with a Cu-H bond of 1.661 Å. The distance between the α-C and H is 1.960 Å. For the products, the CH_3CHOH forms a bond with Cu and the length of this Cu-C bond is 2.073 Å. The dissociated H atom is adsorbed on the hollow site of Cu atoms. The Cu-H bond lengths are 1.799/1.703/1.690 Å.

The reaction barrier on $Cu_3Au(111)$ (Fig.4) was found to be 1.38 eV and the reaction energy to be 1.14 eV. The configuration of ethanol on the $Cu_3Au(111)$ surface also remains the same as that in the O-H cleavage. For the transition state, the H is adsorbed on the hollow site of Cu atoms. The lengths of these Cu-H bonds are 1.770/1.799/1.649 Å. The CH_3CHOH species does not form a strong bond and the distance between the Cu and α-C is 2.545 Å. For the products, the dissociated H atom is still located on the hollow site of Cu atoms and the Cu-H bond lengths are 1.713/1.715/1.790 Å. The CH_3CHOH species is co-adsorbed on one of the three Cu atoms and the Cu-C bond is 2.032 Å.

It can be clearly seen in Fig. 4 that alloying Zr to form Cu_3Zr enhances the catalytic activities in breaking the α-C-H bond when alloying with In, Ag, and Au does not. The activity of $Cu_3Ag(111)$ is slightly better than those of $Cu_3In(111)$ and $Cu_3Au(111)$, but it is still worse than that of Cu(111).

A comparison of O-H and α-C-H bond cleavages in CH_3CH_2OH on all four alloying catalysts: Cu_3Zr, Cu_3In, Cu_3Ag, and Cu_3Au can be made with the results summarized in Table 2. As we mentioned above, $Cu_3Zr(111)$ is a remarkable catalyst for ethanol dehydrogenation reactions of either *o*-H or α-H, since the reaction barriers are both rather low, especially for the O-H bond cleavage (0.13 eV). This indicates that both dehydrogenation channels will be assessable during reaction dynamics.[111] Conversely, $Cu_3In(111)$ and $Cu_3Au(111)$ alloys do not improve dehydrogenation reactions for *o*-H and α-H atoms, since the reaction barriers are all around 1.00-1.40 eV, where some are even strongly endothermic, meaning that dehydrogenation reactions could barely take place around 100℃ on $Cu_3In(111)$ and $Cu_3Au(111)$ surfaces. On the other hand, it can be concluded through comparison that all of the alloy catalysts exhibit better activity in selectively breaking the O-H bond of ethanol than to break the α-C-H bond, while the opposite holds true for Pt and Pd alloys. Though the reaction barriers are lower on the surfaces, Cu_3Pt and Cu_3Pd favor more α-C-H bond breakage[13] followed by the O-H bond cleavage in CH_3CHOH species.[112]

Compared with Cu(111), $Cu_3Zr(111)$ shows more desirable selectivity of the prior dehydrogenation of ethanol, since the difference of reaction barrier energies between the O-H and α-C-H bond cleavage on $Cu_3Zr(111)$ is much larger than that on Cu(111). $Cu_3Ag(111)$, on the other hand, does not present this excellent catalytic performance. Furthermore, significantly

easy access to the product CH_3CH_2O on $Cu_3Zr(111)$ may indicate the main reason for the wide application of ZrO_2 in the one-step dehydrogenation of ethanol to ethyl acetate in which Zr-Cu alloy form may be responsible for the high catalytic activities[113, 114] and since CH_3CH_2O is always the key intermediate in that reaction networks related to the Colley mechanism.[115]

Table 2 Reaction barriers (ΔE_a^0), reaction energies (ΔE^0), and the only imaginary frequency (υ) of each transition state of the O-H and α-C-H bond cleavage reactions on $Cu_3X(111)$ (X=Zr, In, Ag, Au).

$Cu_3X(111)$	**O-H Bond Cleavage**		**υ (cm^{-1})**	**α-C-H Bond Cleavage**		**υ (cm^{-1})**
	ΔE_a^0 (eV)	**ΔE^0 (eV)**		**ΔE_a^0 (eV)**	**ΔE^0 (eV)**	
$Cu(111)$[13]	0.98	-0.01	1242i	0.89	0.73	140i
$Cu_3Zr(111)$	0.13	-1.17	1157*i*	0.73	0.34	944*i*
$Cu_3In(111)$	1.08	0.69	956*i*	1.38	1.17	810*i*
$Cu_3Ag(111)$	0.81	-0.26	1024*i*	1.08	0.78	595*i*
$Cu_3Au(111)$	1.02	-0.19	261*i*	1.38	1.14	236*i*

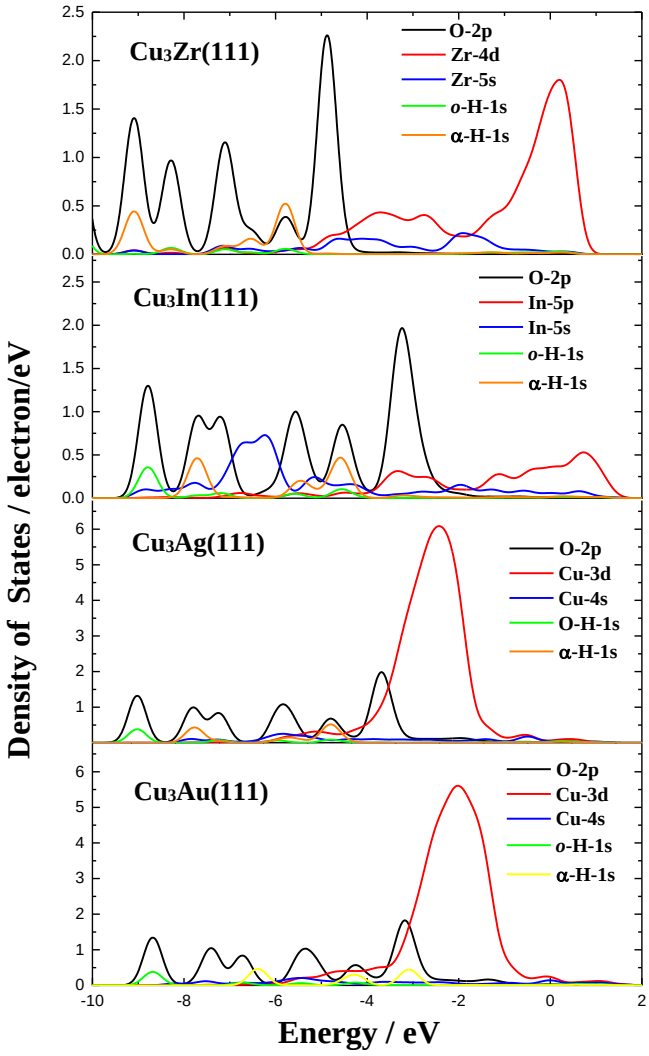

Fig. 5 PDOS analysis (after adsorption) on 2p-orbital of O atom, 1s-orbital of *o*-H atom, and 1s-orbital of α-H atom in ethanol and d-orbital and s-orbital of adsorption center atoms on $Cu_3X(111)$ surfaces (X=Zr, In, Ag, Au).

Furthermore, we can investigate the adsorption process of ethanol from the PDOS profile analysis, which has been used to understand bonding aspects of the adsorbed species.[102, 116-119] PDOS analysis shown in Fig.5 includes the main adsorption center atom exposed to ethanol on the surface, which aims to analyze the electronic structure of adsorption configurations of ethanol. It can be clearly seen through all the PDOS profiles that the adsorption of ethanol on alloy surfaces is basically formed by the 2p-orbital of O atom, the 4d-orbital and the 5s-orbital of Zr atom on $Cu_3Zr(111)$, or 5p-orbital and 5s-orbital of the In atom on $Cu_3In(111)$, or the 4s-orbital and the 3d-orbital of Cu atom on $Cu_3Ag(111)$ and $Cu_3Au(111)$. But for $Cu_3X(111)$ (X= Zr, Ag,

Au), the outermost d-orbital of the Zr atom or Cu atom plays the most essential role during the adsorption process, but for $Cu_3In(111)$, the outermost p-orbital of the In atom is crucial for the adsorption bond of ethanol instead. It is mainly because In is a basic metal rather than a transition metal, and the 4d-orbital of In is not actively involved during the adsorption and the reaction process. Besides, the 4d-orbital of Zr atom on $Cu_3Zr(111)$ crosses the Fermi level, but when it comes to the 3d-orbitals of Cu atoms on $Cu_3X(111)$ (X= Ag, Au), there is nearly no electron distribution around Fermi level, which is able to explain the higher reactivity for dehydrogenation on $Cu_3Zr(111)$ since metal Zr owns more redox capability than Cu does.[120]

A further in-depth explanation of dehydrogenation reactivity on different surfaces can be illustrated partially through Mülliken charge analysis. Figure 6 shows the Mülliken charge differences for the *o*-H atom, α-H atom and O atom in ethanol after and before adsorption on $Cu_3X(111)$ (X= Zr, In, Ag, Au). Fig. 6 also depicts the reaction barriers for correlation purposes. It can be clearly seen that the trend of Mülliken charge differences of different sorts of H atoms and reaction barrier energies of different types of dehydrogenation have a close relationship. Firstly, by taking the *o*-H dehydrogenation as an example, the Mülliken charge of the *o*-H atom in ethanol changes mostly (0.037 electron) when adsorbed on $Cu_3Zr(111)$, which means that the O-H bond is activated mostly on $Cu_3Zr(111)$ surface. This charge transfer is the main reason that the reaction barrier on $Cu_3Zr(111)$ is the lowest. Then, Mülliken charge differences can be arranged from $Cu_3Au(111)$, $Cu_3In(111)$ to $Cu_3Ag(111)$ (0.026 > 0.020 > 0.007). However, the reactivity among them does not completely follow this trend. The dehydrogenation reaction on $Cu_3Ag(111)$ turns out to be much easier, followed by $Cu_3Au(111)$ and $Cu_3In(111)$ (reaction barrier: 0.81 eV < 1.02 eV < 1.08 eV). This trend can be further explained from another aspect

of alloy surface electronic distribution. Because of the difference in electronegativity between Cu and the second alloyed metal X, the surface electronic distribution can turn to be drastically different. The Mülliken charge distribution of the Cu atom and the second alloyed metal X on $Cu_3X(111)$ (X= Zr, In, Ag, Au) can shield some light on the understanding of the catalytic activities. The Cu atoms on $Cu_3Zr(111)$ and $Cu_3Ag(111)$ surfaces have more electron density, since the Mülliken charges of the Cu atom are -0.224 and -0.008 electrons, respectively. The product H atoms in dehydrogenation reactions are finally adsorbed stably on hollow or bridge sites of Cu atoms. Hence, more electron density around Cu atoms can be beneficial for the dehydrogenation reaction to occur. This rule can be reflected on $Cu_3Zr(111)$ and $Cu_3Ag(111)$ surfaces, which may also explain a better O-H bond cleavage reactivity on $Cu_3Ag(111)$ than that on $Cu_3Au(111)$ or $Cu_3In(111)$, though the Cu atom on $Cu_3Ag(111)$ surface does not really activate the O-H bond. Meanwhile, when it comes to the α-C-H bond cleavage, it can also be seen that α-C-H bond breaking occurs much more easily on $Cu_3Zr(111)$ and $Cu_3Ag(111)$ than on $Cu_3Au(111)$ and $Cu_3In(111)$, which means that the rule of surface electronic distribution mentioned above still applies.

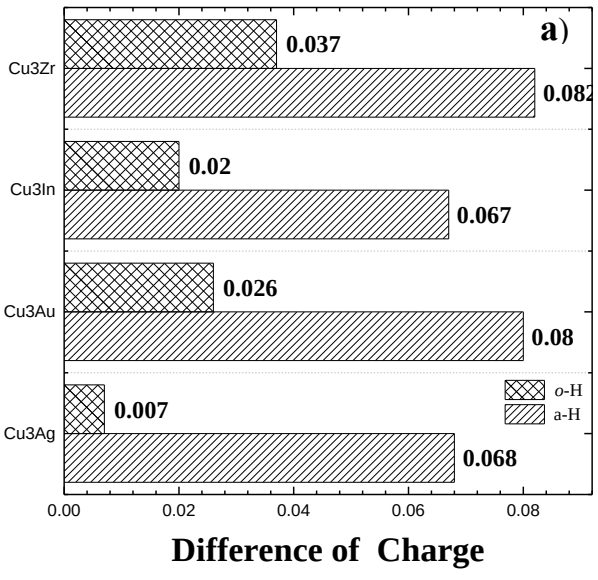

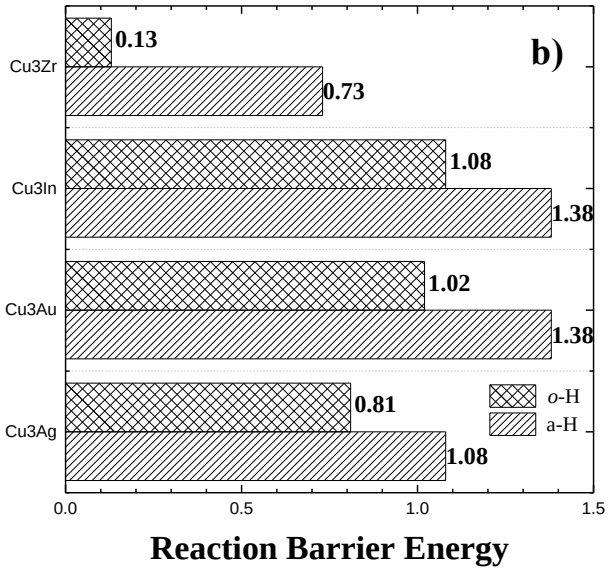

Fig. 6 a) Absolute values of differences of Mülliken charge of *o*-H atom and α-H atom in ethanol after and before adsorption on $Cu_3X(111)$ (X= Zr, In, Ag, Au) (electron). b) Reaction barrier energies of *o*-H and α-H dehydrogenation reactions on $Cu_3X(111)$ (X= Zr, In, Ag, Au) (eV).

Dehydrogenation reactions of ethanol on $Cu_3X(111)$ (X= Zr, In, Ag, Au) are closely associated with d-band centers of different reaction center atoms on the surfaces.[120] In Fig.7(a, b) PDOS profiles of d-orbitals and d-band centers of different atoms are presented (Note: For In, it is p-orbital). It can be clearly seen that the d-band center of the Zr atoms on $Cu_3Zr(111)$ is much closer to the Fermi level than others, which means that the reaction center Zr features better activity for dehydrogenation reactions than the other metals. In is different from other metals, since metal In is not a transition metal. The outermost p-orbital of In atom is mostly involved in dehydrogenation reactions. It can be clearly seen that the p-band center is also close to the Fermi level, just like the d-band center of Zr atom, but the reactivity on In atom is still quite low, which means that the p-orbital does not exhibit comparable ability with the d-orbital in dehydrogenation. When alloyed with Zr and In, the d-band centers of Cu atoms on $Cu_3Zr(111)$ and $Cu_3In(111)$ move away from Fermi level compared with Cu(111). As for $Cu_3Ag(111)$ and $Cu_3Au(111)$, it can be concluded that the d-band centers of the Cu atoms,

when alloyed with Ag and Au, move closer to the Fermi level when compared with Cu(111). Meanwhile, the d-band centers of Cu atoms on $Cu_3Ag(111)$ and $Cu_3Au(111)$ are basically the same, and the former one is a little bit smaller than the later one (-2.25 eV < -2.22 eV). However, the peak of density of states of d-orbital of Cu atoms on $Cu_3Ag(111)$ is higher than that on $Cu_3Au(111)$, which is consistent with the results of more electron density occupied around Cu atoms on $Cu_3Ag(111)$ mentioned above. This could be the main reason that prior dehydrogenation reactions can occur more easily on $Cu_3Ag(111)$ than $Cu_3Au(111)$. Besides, through Fig.7c, it can be clearly seen that the DOS profile of $Cu_3In(111)$ is greatly different from other profiles, since it is more non-localized and has a significant peak of density of states around approximately -15 eV, which further explains its poor activity. DOS profiles of $Cu_3Ag(111)$ and $Cu_3Au(111)$ are pretty similar, and other than the highest peak around -2.5 eV, there are other small peaks of density of states around -5 eV in these profiles, which may be attributed to Ag and Au atoms in the bulk system. Besides, for $Cu_3Zr(111)$, another significant small peak of density of states is located across the Fermi level due to Zr atoms in the bulk, which meets the agreement with the results mentioned above.

Table 3 The d/p-band centers of different atoms on $Cu_3X(111)$ (X= Zr, In, Ag, Au) (For In, it is p-orbital) and pure Cu(111) surface (eV).

$Cu_3X(111)$	**$Cu_3Zr(111)$**	**$Cu_3In(111)$**	**$Cu_3Ag(111)$**	**$Cu_3Au(111)$**	**Cu(111)**
d-band Cu	-2.78	-2.55	-2.25	-2.22	-2.40
d/p-band X	-1.10	-1.16	-4.19	-3.83	—

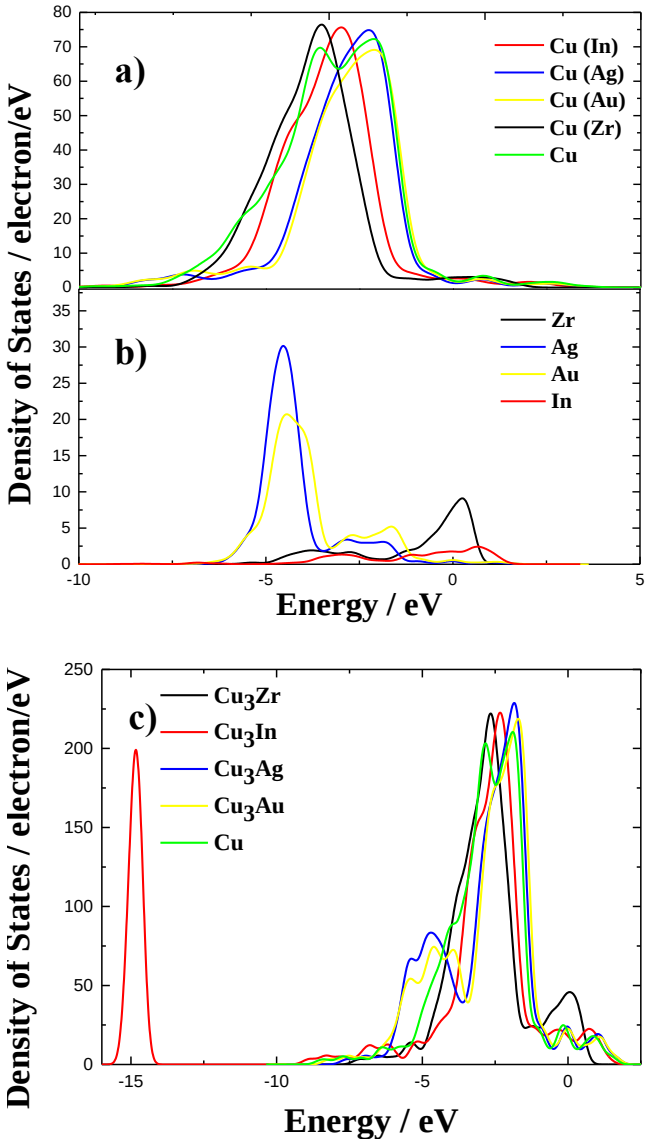

Fig.7 a) PDOS profiles of d-orbitals Cu atoms on Cu(111) and Cu_3X(111) bare surface (X= Zr, In, Ag, Au). b) PDOS profiles of d/p-orbitals X atoms on Cu_3X(111) bare surface (X= Zr, In, Ag, Au) (For In, it is p-orbital). c) DOS profiles of bulk Cu_3X and Cu (X= Zr, In, Ag, Au).

Overall, it can be clearly seen that there are two major factors that can significantly influence the reactivity of prior dehydrogenation reactions, or even the type of dehydrogenation reactions. Compared with the results on Cu(111), or Cu_3Pd(111) and Cu_3Pt(111), where α-C-H bond cleavage is competitive with O-H bond cleavage, all the alloy surfaces mentioned above make the O-H bond cleavage of ethanol more accessible and energetically favorable. Some alloys were successful at reducing reaction barriers of the first dehydrogenation of ethanol signifi-cantly, which may be attributed to the specific properties of the second metal X, which can

directly activate the O-H bond of ethanol or indirectly change the d-band center of Cu atoms and surface lattice parameters. Other than that, surface electronic distribution effect cannot be ignored, since the significant differences in electronegativity can create an obvious acid-base position on the surfaces, and more electronic density around the Cu atoms where H atoms can be stably adsorbed can greatly promote the reactivity of dehydrogenation reactions on alloy catalyst surfaces. These two factors mutually and coherently influence the prior dehydrogenation reactions.

Brønsted–Evans–Polanyi (BEP) has been applied in a great volume of research.[114, 121, 122] Here, the BEP relationships of the O-H bond and α-C-H bond cleavages, including $Cu_3X(111)$ (X=Zr, In, Ag, Au, Pt, Pd) and Cu(111),[13] are presented in Fig.8. For the O-H bond cleavage, the BEP relationship is y (eV)=0.555x (eV)+0.917, and R^2 =0.780, and for the α-C-H bond cleavages, the BEP relationship is y (eV)=0.987x (eV)+0.225, and R^2 =0.880. The BEP relationship may better describe the α-C-H bond cleavage reaction in ethanol. A proper linear BEP relationship always means that reaction barrier energies are mostly associated with electronic properties of chemical bonds in reactants. Hence, there may be more specific factors other than the electronic effect that can influence the barrier energies of the O-H bond cleavage on different surfaces. We can predict the reaction barriers of α-C-H bond cleavage to some extent by analyzing the configurations of FS and IS on different surfaces. For the O-H bond breaking, this correlation may provide some insights into the trend of this elementary step on a series of metals, though the configurations of FS and IS cannot directly determine the reaction barriers.

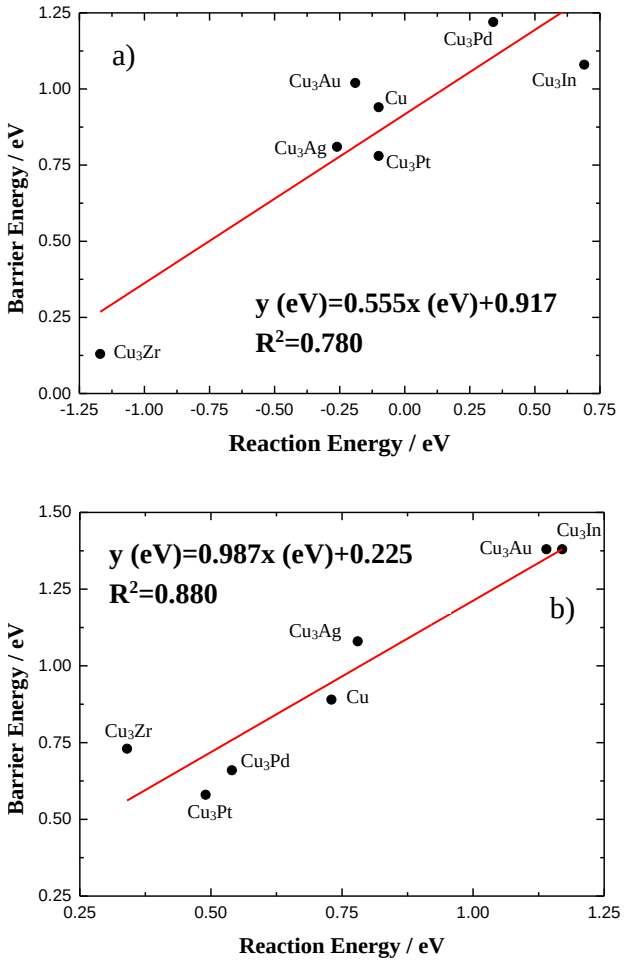

Fig. 8 a) BEP relationship between reaction barrier energies and reaction energies of the O-H bond cleavage. b) BEP relationship between reaction barrier energies and reaction energies of the α-C-H bond cleavage.

Conclusions

In this study, O-H and α-C-H bond cleavage reactions of ethanol on $Cu_3X(111)$ (X= Zr, In, Ag, Au) have been studied using DFT. The key reaction centers for dehydrogenation reactions on $Cu_3Zr(111)$ and $Cu_3In(111)$ are metal Zr and In, respectively, and others are metal Cu on $Cu_3Ag(111)$ and $Cu_3Au(111)$. $Cu_3Zr(111)$ exhibits obviously superior catalytic performance among the others with a significantly low reaction barrier for the O-H cleavage reaction (0.13 eV). Although we cannot directly take Cu_3Zr as an ideal catalyst based on our current study, our research can still provide a valuable insight and will stimulate future studies on the CuZr

catalysts for dehydrogenation of ethanol. On all of the alloy surfaces, ethanol is more likely to have the O-H bond breaking instead of the α-C-H bond cleavage, in contrast to the results on Cu(111). The effects on catalytic performances for dehydrogenation reactions on $Cu_3X(111)$ are related to two main factors. Firstly, the specific inherent effects of the second alloy metal X are significant, including its indirect effects on the d-band center of the metal Cu, since its adsorption and activation of ethanol or H atoms may reduce the reaction barrier energies effectively. Secondly, electronic distribution on the surfaces, due to the differences in electronegativity between Cu and the second alloyed metal X, is also important since greater electron density occupied around Cu atoms on surfaces is beneficial for the adsorption of H atoms, especially when H atoms can be adsorbed more stably on the sites of Cu atoms, and can also reduce the reaction barrier energies to some extent.

Since the second alloyed metal have shown great effects on the selective dehydrogenation reactions of ethanol, these encouraging results will serve as a great starting point for future studies. The future work includes the investigations of optimal composition of Zr in CuZr alloyed catalysts and the second dehydrogenation, i.e. CH3CH2O → CH3CH=O, to form aldehyde and desorption of aldehyde on the optimal CuZr catalyst. Further exploration of the synergistic effects of alloying will also be interesting.

Conflicts of interest

The authors declare no competing financial interest.

Corresponding Authors:
L. Wang: lwang@chem.siu.edu

Acknowledgements

This work was supported by the Tianjin Science and Technology Council. LW acknowledges the sabbatical program at Southern Illinois University.

References

1. M. A. F. Akhairi and S. K. Kamarudin, *Int. J. Hydrog. Energy*, 2016, **41**, 4214-4228.
2. M. Z. F. Kamarudin, S. K. Kamarudin, M. S. Masdar and W. R. W. Daud, *Int. J. Hydrog. Energy*, 2013, **38**, 9438-9453.
3. A. Rodriguez-Gomez, J. P. Holgado and A. Caballero, *ACS Catal.*, 2017, **7**, 5243-5247.
4. A. Haryanto, S. Fernando, A. Naveen Murali and S. Adhikari, *Energy Fuels*, 2005, **19**, 2098-2106.
5. R. M. Navarro, M. A. P. And and J. L. G. Fierro, *Chem. Rev.*, 2007, **107**, 3952.
6. S. S. Munjewar, S. B. Thombre and R. K. Mallick, *Renewable Sustainable Energy Rev.*, 2017, **67**, 1087-1104.
7. R. Wu and L. Wang, *J. Phys. Chem. C* 2022, **126**, 21650-21666.
8. R. Wu and L. Wang, *Chem. Phy. Lett.*, 2017, **678**, 196-202.
9. K. Sun, M. Zhang and L. Wang, *Chem. Phys. Lett.*, 2013, **585**, 89-94.
10. L. Yaqoob, T. Noor and N. Iqbal, *RSC Adv.*, 2021, **11**, 16768-16804.
11. K. Inui, T. Kurabayashi and S. Sato, *J. Mol. Catal. A: Chem.*, 2002, **237**, 53-61.
12. A. B. Sánchez, N. Homs, J. L. G. Fierro and P. R. D. L. Piscina, *Catal. Today*, 2005, **s 107–108**, 431-435.
13. A. B. Gaspar, F. G. Barbosa, S. Letichevsky and L. G. Appel, *Appl. Catal. A*, 2010, **380**, 113-117.
14. R. Wu and L. Wang, *J. Phys. Chem. C*, 2020, **124**, 26953-26964.
15. Z.-P. Wu, B. Miao, E. Hopkins, K. Park, Y. Chen, H. Jiang, M. Zhang, C.-J. Zhong and L. Wang, *J. Phys. Chem. C*, 2019, **123**, 20853-20868.
16. G. L. Zhao, C. H. Fang, J. W. Hu and D. L. Zhang, *ChemPlusChem*, 2021, **86**, 574-586.
17. M. Wala and W. Simka, *Molecules*, 2021, **26**, 2144.
18. R. Rizo, A. Bergmann, J. Timoshenko, F. Scholten, C. Rettenmaier, H. S. Jeon, Y.-T. Chen, A. Yoon, A. Bagger, J. Rossmeisl and B. R. Cuenya, *J. Catal.*, 2021, **393**, 247-258.
19. S. G. Peera, C. Liu, J. Shim, A. K. Sahu, T. G. Lee, M. Selvaraj and R. Koutavarapu, *Ceramics Int.*, 2021, **47**, 28106-28121.
20. N. S. Mohd-Nasir, O. U. Osazuwa and S. Z. Abidin, *Int. J. Hydrog. Energy*, 2021, **46**, 31000-31023.
21. D. Martín-Yerga, G. Henriksson and A. Cornell, *Int. J. Hydrog. Energy*, 2021, **46**, 1615−1626.
22. S. Luo, L. Zhang, Y. Liao, L. Li, Q. Yang, X. Wu, X. Wu, D. He, C. He, W. Chen, Q. Wu, M. Li, E. J. M. Hensen and Z. Quan, *Adv. Mater.*, 2021, **33**, 2008508.
23. X. Zhao, Q. Liu, Q. Li, L. Chena, L. Mao, H. Wang and S. Chen, *Chem. Eng. J.*, 2020, **400**, 125744.
24. J. Zhang, S. F. Lu, Y. Xiang and S. P. Jiang, *ChemSusChem*, 2020, **13**, 2484-2502.
25. S. Bepari and D. Kuila, *Int. J. Hydrog. Energy*, 2020, **45**, 18090-18113.
26. C. Zhu, B. Lan, R.-L. Wei, C.-N. Wang and Y.-Y. Yang, *ACS Catal.*, 2019, **9**, 4046-4053.
27. B. C. Yang, J. Koo, J. W. Shin, D. Go, J. H. Shim and J. An, *Energy Technol.*, 2019, **7**, 5-19.
28. M. Taghizadeh and F. Aghili, *Rev. Chem. Eng.*, 2019, **35**, 377-392.
29. L. Rossner and M. Armbruster, *ACA Catal.*, 2019, **9**, 2018-2062.
30. R. Rizo, S. Perez-Rodriguez and G. Garcia, *ChemElectroChem*, 2019, **6**, 4725-4738.

31. A. R. Poerwoprajitno, L. Gloag, S. Cheong, J. J. Gooding and R. D. Tilley, *Nanoscale*, 2019, **11**, 18995-19011.
32. S. G. Peera, T. G. Lee and A. K. Sahu, *Sustain. Energy Fuels*, 2019, **3**, 1866-1891.
33. N. S. Marinkovic, M. Li and R. R. Adzic, *Topics Current Chem.*, 2019, **377**, 11.
34. J. Bai, D. Y. Liu, J. Yang and Y. Chen, *ChemSusChem*, 2019, **12**, 2117-2132.
35. Y. C. Sharma, A. Kumar, R. Prasad and S. N. Upadhyay, *Renew. Sustain. Energy Rev.*, 2017, **74**, 89-103.
36. E. A. Monyoncho, S. N. Steinmann, C. Michel, E. A. Baranova, T. K. Woo and P. Sautet, *ACS Catal.*, 2016, **6**, 4894-4906.
37. R. M. Altarawneh, *Energy Fuels*, 2021, **35**, 11594-11612.
38. S. Nanda, R. Rana, Y. Zheng, J. A. Kozinski and A. K. Dalai, *Sustain. Energy Fuels*, 2017, **1**, 1232-1245.
39. R. Wu and L. Wang, *ChemPhysChem*, 2022, e202200132.
40. R. Wu and L. Wang, *Chem. Phys. Impact*, 2021, **3**, 100040.
41. M. Li, W. Guo, R. Jiang, L. Zhao and H. Shan, *Langmuir*, 2010, **26**, 1879-1888.
42. H. F. Wang and Z. P. Liu, *J. Am. Chem. Soc.*, 2008, **130**, 10996-11004.
43. L. Xiao and L. Wang, *J. Phys. Chem. A*, 2004, **108**, 8605-8614.
44. L. Huang, S. Zaman, Z. T. Wang, H. T. Niu, B. You and B. Y. Xia, *Acta Physico-Chimica Sinica*, 2021, **37**, 2009035.
45. X. F. Ren, Q. Y. Lv, L. F. Liu, B. H. Liu, Y. R. Wang, A. M. Liu and G. Wu, *Sustainable Energy Fuels*, 2020, **4**, 15-30.
46. B. W. Zhang, H. L. Yang, Y. X. Wang, S. X. Dou and H. K. Liu, *Adv. Energy Mater.*, 2018, **8**, 1703597.
47. Y. Liu, M. Wei, D. Raciti, Y. Wang, P. Hu, J. H. Park, M. Barclay and C. Wang, *ACS Catal.*, 2018, **8**, 10931-10937.
48. F. D. Liu, H. L. Wang, A. Sapi, H. Tatsumi, D. Zherebetskyy, H. L. Han, L. M. Carl and G. A. Somorjai, *Catalysts*, 2018, **8**, 226.
49. S. B. Duan, Z. Du, H. S. Fan and R. M. Wang, *Nanomater.*, 2018, **8**, 949.
50. J. Wang, B. Li, T. Yersak, D. J. Yang, Q. F. Xiao, J. L. Zhang and C. Zhang, *J. Mater. Chem. A*, 2016, **4**, 11559-11581.
51. W. Zhang, Q. Ge and L. Wang, *J. Chem. Phys.*, 2003, **118**, 5793-5801.
52. S. M. Han and C. B. Mullins, *Acc. Chem. Res.*, 2021, **54**, 379-387.
53. S. M. Han, C. H. He, Q. B. Yun, M. Y. Li, W. Chen, W. B. Cao and Q. P. Lu, *Coord. Chem. Rev.*, 2021, **445**, 214085.
54. X. Yang, Z. Liang, S. Chen, M. Ma, Q. Wang, X. Tong, Q. Zhang, J. Ye, L. Gu and N. Yang, *Small*, 2020, **16**, 2004727.
55. N.-F. Yu, N. Tian, Z.-Y. Zhou, T. Sheng, W.-F. Lin, J.-Y. Ye, S. Liu, H.-B. Ma and S.-G. Sun, *ACS Catal.*, 2019, **9**, 3144-3152.
56. E. A. Monyoncho, S. N. Steinmann, C. Michel, E. A. Baranova, T. K. Woo and P. Sautet, *ACS Catal.*, 2016, **6**, 4894-4906.
57. J. Lu, C. Aydin, N. D. Browning, L. Wang and B. C. Gates, *Catal. Lett.*, 2012, **142**, 1445-1451.
58. Q. Chang, S. Kattel, X. Li, Z. Liang, B. M. Tackett, S. R. Denny, P. Zhang, D. Su, J. G. Chen and Z. Chen, *ACS Catal.*, 2019, **9**, 7618-7625.
59. L. Xiao, B. Tollberg, X. Hu and L. Wang, *J. Chem. Phys.*, 2006, **124**, 114309.
60. K. Spivey, J. I. Williams and L. Wang, *Chem. Phys. Lett.*, 2006, **432**, 163-166.
61. C. J. Li, O. J. H. Chai, Q. F. Yao, Z. H. Liu, L. Wang, H. J. Wang and J. P. Xie, *Mater. Horizons*, 2021, **8**, 1657-1682.

62. F. L. Lyu, M. H. Cao, A. Mahsud and Q. Zhang, *J. Mater. Chem. A*, 2020, **8**, 15445-15457.
63. Y. H. Hui, S. W. Zhang and W. T. Wang, *Adv. Syn. Catal.*, 2019, **361**, 2215-2235.
64. H. Xu, B. Miao, M. Zhang, Y. Chen and L. Wang, *Phys. Chem. Chem. Phys.*, 2017, **19**, 26210-26220.
65. M. Ammam and E. B. Easton, *J. Power Sources*, 2013, **222**, 79-87.
66. F. Munoz, C. Hua, T. Kwong, L. Tran, T. Q. Nguyen and J. L. Haan, *Appl. Catal. B*, 2015, **s 174–175**, 323-328.
67. J. Noborikawa, J. Lau, J. Ta, S. Hu, L. Scudiero, S. Derakhshan, H. Su and J. L. Haan, *Electrochimica Acta*, 2014, **137**, 654-660.
68. J. Yin, S. Shan, M. S. Ng, L. Yang, D. Mott, W. Fang, N. Kang, J. Luo and C. J. Zhong, *Langmuir*, 2013, **29**, 9249.
69. D. P. Volanti, A. G. Sato, M.O. Orlandi. J.M.C. Bueno, E.Longo, and J. Andrés, *ChemCatChem*, 2011, **3**, 839–843.
70. F. W. Chang, W. Y. Kuo and K. C. Lee, *Appl. Catal. A*, 2003, **246**, 253-264.
71. Z.-T. Wang, Y. Xu, M. El-Soda, F. R. Lucci, R. J. Madix, C. M. Friend and E. C. H. Sykes, *J. Phys. Chem. C*, 2017, **121**, 12800-12806.
72. X. Fan, Z. Wu, L. Wang and C. Wang, *Chem. Mater.*, 2017, **29**, 639.
73. S. R. Bheemireddy, P. C. Ubaldo, A. D. Finke, L. Wang and K. N. Plunkett, *J. Mater. Chem. C*, 2016, **4**, 3963-3969.
74. B. Yuan, J. Zhuang, K. M. Kirmess, C. N. Bridgmohan, A. C. Whalley, L. Wang and K. N. Plunkett, *J. Org. Chem.*, 2016, **81**, 8312-8318.
75. L. Lu, S. Zou and B. Fang, *ACS Catal.*, 2021, **11**, 6020-6058.
76. J. Sun, A. M. Karim, D. Mei, M. Engelhard, X. Bao and Y. Wang, *Appl. Catal. B,* 2015, **162**, 141-148.
77. J. Agrell, H. Birgersson, M. Boutonnet, I. Melián-Cabrera, R. M. Navarro and J. L. G. Fierro, *J. Catal.*, 2003, **219**, 389-403.
78. M. Shimokawabe, H. Asakawa and N. Takezawa, *Appl. Catal.*, 1990, **59**, 45-58.
79. J. M. Hidalgo, Z. Tišler, R. Bulánek, P. Čičmanec, K. Raabová and D. Kubička, *React. Kinet, Mecha Catal.*, 2017, **121**, 161-173.
80. W. P. Xiao, W. Lei, M. X. Gong, H. L. Xin and D. L. Wang, *ACS Catal.*, 2018, **8**, 3237-3256.
81. M. Tang, D. Zhao, M. Pan and W. Wang, *Chin. Phys. Lett.*, 2004, **21**, 901.
82. S. Pauly, S. Gorantla, G. Wang, U. Kühn and J. Eckert, *Nat. Mater.*, 2010, **9**, 473.
83. G. Onyestyák, S. Harnos and D. Kalló, *Catal. Commun.*, 2012, **26**, 19-24.
84. G. Onyestyák, S. Harnos, S. Klébert, M. Štolcová, A. Kaszonyi and D. Kalló, *Appl. Catal. A*, 2013, **s 464–465**, 313-321.
85. G. Onyestyák, S. Harnos, M. Štolcová, A. Kaszonyi and D. Kalló, *Catal. Commun.*, 2013, **40**, 32-36.
86. G. Onyestyák, S. Harnos, C. A. Badari, E. Drotár, S. Klébert and D. Kalló, *Open Chem.*, 2014, **13**.
87. J. Liu, H. Lyu, Y. Chen, G. Li, H. Jiang and M. Zhang, *Phys. Chem. Chem. Phys.*, 2017, **19**, 28083-28097.
88. E. L. Clark, C. Hahn, T. F. Jaramillo and A. T. Bell, *J. Am. Chem. Soc.*, 2017, **139**, 15848-15857.
89. S. Verma, R. B. Nasir Baig, M. N. Nadagouda and R. S. Varma, *ACS Sustainable Chem. Eng.*, 2017, **5**, 3637-3640.
90. R. E. Ramírez-Garza, I. Rodríguez-Iznaga, A. Simakov, M. H. Farías and F. F. Castillón-Barraza, *Mater. Res. Bull.*, 2018, **97**, 369-378.
91. E. A. Redina, A. A. Greish, I. V. Mishin, G. I. Kapustin, O. P. Tkachenko, O. A. Kirichenko and L. M. Kustov, *Catal. Today*, 2015, **241**, 246-254.
92. D. T. Mai, A. I. Pylinina and I. I. Mikhailenko, *Russian J. Phys. Chem. A*, 2015, **89**, 1184-1188.

93. B. Delley, *J. Chem. Phys.*, 1990, **92**, 508-517.
94. B. Delley, *J. Phys. Chem.*, 1996, **100**, 6107-6110.
95. J. P. Perdew, K. Burke and M. Ernzerhof, *Generalized Gradient Approximation Made Simple*, 1996.
96. B. Miao, Z. Wu, H. Xu, M. Zhang, Y. Chen and L. Wang, *Chem. Phys. Lett.*, 2017, **688**. 92-97.
97. D. R. Lide, *CRC Handboook of Chemistry and Physics*, CRC Press, 1985.
98. R. A. Hoyt, M. M. Montemore, E. C. H. Sykes and E. Kaxiras, *J. Phys. Chem. C*, 2018, **122**, 21952-21962.
99. Z.-P. Wu, S. Shan, Z.-H. Xie, N. Kang, K. Park, E. Hopkins, S. Yan, A. Sharma, J. Luo, J. Wang, V. Petkov, L. Wang and C.-J. Zhong, *ACS Catal.*, 2018, **8**, 11302-11313.
100. W. Zhang and L. Wang, *Comput. Theor. Chem.*, 2011, **963**, 236-244.
101. S. Grimme, A. Hansen, J. G. Brandenburg and C. Bannwarth, *Chem. Rev.*, 2016, **116**, 5105-5154.
102. C. Wu, L. Wang, Z. Xiao, G. Li and L. Wang, *Chem. Phys. Lett.*, 2020, **746**, 137229.
103. S. Verma, R. B. N. Baig, M. N. Nadagouda and R. S. Varma, *ACS Sustainable Chem. Eng.*, 2017, **5**, 3637-3640.
104. K. Y. Liu, J. Liu and J. M. Herbert, *J. Comput. Chem.*, 2017, **38**, 1678-1684.
105. H. Xu, B. Miao, M. Zhang, Y. Chen and L. Wang, *Phys. Chem. Chem. Phys.*, 2017, **19**, 26210.
106. Z. Wu, M. Zhang, H. Jiang, C. J. Zhong, Y. Chen and L. Wang, *Phys. Chem. Chem. Phys.*, 2017, **19**, 15444-15453.
107. B. Miao, Z.-P. Wu, M. Zhang, Y. Chen and L. Wang, *J. Phys. Chem. C*, 2018, **122**, 22448-22459.
108. R. Wu, K. R. Wiegand, L. Ge and L. Wang, *J. Phys. Chem. C* 2021, **125**, 14275-14286.
109. L. Wang, J. I. Williams, T. Lin and C. J. Zhong, *Catal. Today*, 2011, **165**, 150-159.
110. Z. F. Xu and Y. Wang, *J. Phys. Chem.. C*, 2011, **115**, 20565-20571.
111. L. Wang, C. Kalyanaraman and A. B. McCoy, *J. Chem. Phys.*, 1999, **110**, 11221-11232.
112. R. Wu and L. Wang, *Comput. Mater. Sci.*, 2021, **196**, 110514.
113. A. G. Sato, D. P. Volanti, D. M. Meira, S. Damyanova, E. Longo and J. M. C. Bueno, *J. Catal.*, 2013, **307**, 1-17.
114. J. E. Sutton and D. G. Vlachos, *ACS Catal.*, 2012, **2**, 1624–1634.
115. S. W. Colley, J. Tabatabaei, K. C. Waugh and M. A. Wood, *J. Catal.*, 2005, **236**, 21-33.
116. C. Wu, Z. Xiao, L. Wang, G. Li, X. Zhang and L. Wang, *Catal. Sci. Technol.*, 2021, **11**, 1965-1973.
117. R. Wu, K. R. Wiegand and L. Wang, *J. Chem. Phys.*, 2021, **154**, 054705.
118. R. Wu, K. Sun, Y. Chen, M. Zhang and L. Wang, *Surf. Sci.*, 2021, **703**, 121742.
119. B. Miao, Z.-P. Wu, H. Xu, M. Zhang, Y. Chen and L. Wang, *Comput. Mater. Sci.*, 2019, **156**, 175-186.
120. J. H. Wang, C. S. Lee and M. C. Lin, *J. Phys. Chem. C*, 2009, **113**, 6681-6688.
121. J. E. Sutton and D. G. Vlachos, *Ind. Eng. Chem. Res.*, 2015, **54**, 4213-4225.
122. S. Wang, V. Vorotnikov, J. E. Sutton and D. G. Vlachos, *ACS Catal.*, 2014, **4**, 604–612.